J Adv Ceram

Research Article

Enhancement of densification and mechanical property of $(Hf_{0.2}Zr_{0.2}Ti_{0.2}Nb_{0.2}Ta_{0.2})N$ high-entropy bulk ceramic via silicon carbide addition

Wuyang Song[1], Youjun Lu[1,2,✉], Lutong Yang[1], Maohui Li[1,✉], Xiao Zhang[1], Bo Ma[1], Chuyun Wang[1], Yanmin Wang[1,3], Jinfeng Li[1], Xiang Liu[1]

Cite this article: Song W, Lu Y, Yang L, et al. *J Adv Ceram* 2025, **14**(1): 9221004. https://doi.org/10.26599/JAC.2024.9221004

ABSTRACT: In this work, high-entropy composite bulk ceramic of $(Hf_{0.2}Zr_{0.2}Ti_{0.2}Nb_{0.2}Ta_{0.2})N$/silicon carbide (HEN–SiC) was fabricated via spark plasma sintering (SPS) at 2100 °C with submicron-sized single-phase $(Hf_{0.2}Zr_{0.2}Ti_{0.2}Nb_{0.2}Ta_{0.2})N$ (HEN) powder as a raw material and SiC particles as a sintering aid. The crystal structure, phase composition, and grain size/morphology of the composite were characterized by X-ray diffraction, scanning electron microscopy, transmission electron microscopy, and energy dispersive spectroscopy. The relative density and mechanical properties (i.e., bending strength, Vickers hardness, and fracture toughness) of the composite bulk ceramics were analyzed. The results show that the relative density of the composite bulk ceramics with increasing SiC particle content from 0 to 10.0 wt% increases from 93.08%±0.13% to 99.12%±0.12%. The high-entropy composite bulk ceramic with SiC particle content of 10.0 wt% exhibits the optimum mechanical properties (i.e., Vickers hardness of 23.34±0.67 GPa, fracture toughness of 4.35±0.13 MPa·m$^{1/2}$, and bending strength of 409±11 MPa) compared with the ceramic without SiC particles (i.e., Vickers hardness of 19.16±0.56 GPa, fracture toughness of 3.78±0.09 MPa·m$^{1/2}$, and bending strength of 335±11 MPa). These results indicate that SiC particles can be distributed and fill the HEN grain boundaries in the ceramic matrix, promoting composite densification via pinning grain boundaries and inhibiting grain growth. The enhanced fracture toughness can be due mainly to fine-grain toughening in addition to lamellar/chain structure toughening. The use of SiC as a sintering aid can promote the densification and fracture toughness of high-entropy nitride bulk ceramics, providing a promising approach for the preparation of high-density, high-performance high-entropy nitride bulk ceramics.

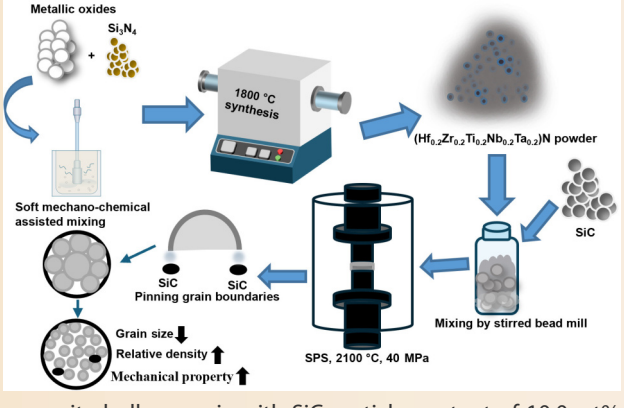

KEYWORDS: high-entropy nitride ceramic; composite ceramic; fine-grain toughening; mechanical properties

1 Introduction

High-entropy ceramics (HECs) are an emerging class of single-phase solid solution ceramic materials composed of multiple near-equimolar principal elements initially reported in 2015 [1]. HECs can be categorized into high-entropy oxide ceramics and high-entropy non-oxide ceramics. High-entropy non-oxide ceramics have broad application prospects in extreme engineering environments, such as aerospace, nuclear energy, and high-speed cutting, because of their superior physical and chemical properties, such as low thermal conductivity, ablation resistance, and ultra-high hardness [2,3]. However, the existing work mainly focuses on the fabrication of high-entropy non-oxide ceramic (i.e., carbide, boride, and nitride) powders via different methods, such as molten salt synthesis [4,5], mechanical alloying [6], self-propagating high-temperature synthesis [7], and soft urea strategy [8,9]. It is thus necessary to develop high-entropy bulk non-oxide ceramics as well as ceramic structural components with high density and superior mechanical properties (i.e., bending strength, hardness, fracture toughness, etc.) by using the related high-entropy ceramic powders. Although there are some studies on high-entropy bulk carbide and boride ceramics, the studies on

[1] School of Materials Science and Engineering, North Minzu University, Yinchuan 750021, China. [2] National and Local Joint Engineering Research Center of Advanced Carbon-Based Ceramics Preparation Technology, Yinchuan 750021, China. [3] College of Materials Science and Engineering, South China University of Technology, Guangzhou 510641, China.

✉ Corresponding authors. E-mail: Y. Lu, youjunlu518@hotmail.com; M. Li, lmnlmb@126.com

Received: September 17, 2024; Revised: October 29, 2024; Accepted: November 17, 2024

high-entropy nitride bulk ceramics are relatively scarce, mainly because of the poor sintering activity of high-entropy nitride ceramic powders during sintering, which affects the densification and mechanical properties of the related bulk ceramics. Liu *et al.* [10] prepared $(Hf_{0.2}Zr_{0.2}Ti_{0.2}Nb_{0.2}Ta_{0.2})N$ bulk ceramics with coarser grains and a lower relative density by a soft mechanochemistry-assisted nitride thermal reduction method with powder. As is known, the sintering of high-entropy bulk ceramics is a complex physical and chemical process, especially concerning the grain growth for densification during sintering [11]. In addition to some intrinsic effects, such as element diffusion mechanism and grain boundary energy, grain growth in high-entropy bulk ceramics can be affected by several dominant factors (i.e., sintering temperature, sintering pressure, and presence of a second phase) [12]. The introduction of a sintering aid (or secondary phase) suitable for the fabrication of high-entropy non-oxide bulk ceramics by sintering is promising for enhancing the densification and mechanical properties via inhibiting the abnormal grain growth. Silicon carbide (SiC) is a commonly used sintering additive or aid in the fabrication of high-entropy bulk ceramics because of its ability to refine grains and improve material properties (i.e., density and mechanical properties) [13–15]. Cheng *et al.* [16] investigated the effect of SiC particles on the densification of high-entropy diboride bulk ceramics, and their results showed that the addition of SiC particles effectively reduced the grain growth rate during sintering. Lu *et al.* [17] fabricated $(Hf_{0.2}Zr_{0.2}Ti_{0.2}Nb_{0.2}Ta_{0.2})C$ composite bulk ceramics with 20 vol% SiC particles via spark plasma sintering (SPS), resulting in superior properties (i.e., density of 99.3%, four-point bending strength of 554±73 MPa, and fracture toughness of 4.51±0.61 $MPa{\cdot}m^{1/2}$). Guo *et al.* [18] prepared $(Hf_{0.2}Zr_{0.2}Ti_{0.2}Nb_{0.2}Ta_{0.2})C$ bulk ceramics via SPS without and with SiC particles as a sintering aid or secondary phase. Their results indicated that the relative density could increase to 97%, and the crack deflection toughening mechanism could be due to the addition of SiC particles during sintering. Rana *et al.* [19] obtained (Zr–Ta–W–Ti)C–SiC composite bulk ceramics with a density of 99.6% via SPS in the presence of SiC particles. Kombamuthu *et al.* [15] increased the density of $(Hf_{0.2}Zr_{0.2}Ti_{0.2}Nb_{0.2}Ta_{0.2})B_2$ bulk ceramics prepared via SPS with SiC particles as a sintering aid. The work described above indicates that high-entropy non-oxide bulk ceramics with a high density and superior mechanical properties could be obtained when SiC particles were used as a sintering aid.

In this work, high-entropy $(Hf_{0.2}Zr_{0.2}Ti_{0.2}Nb_{0.2}Ta_{0.2})N$/silicon carbide (HEN–SiC) composite bulk ceramics were fabricated via SPS at different mass contents of SiC particles as a sintering aid. The effects of SiC particle content on the densification, microstructure, and mechanical properties of HEN–SiC bulk ceramics were investigated. In addition, the mechanisms by which the densification and mechanical properties (i.e., bending strength, hardness and fracture toughness) of the composite bulk ceramics were enhanced in the absence and presence of SiC particles were also analyzed.

2 Experimental

2.1 Materials

In this study, micron-sized powders of HfO_2, ZrO_2, TiO_2, Nb_2O_5, Ta_2O_5, and Si_3N_4 with particle sizes of 1–5 μm and purity of 99.9% (Shanghai Aladdin Biochemical Tech. Co., Ltd., China) were used as raw materials for the synthesis of high-entropy nitride ceramics, and micron-sized powder of α-SiC with a particle size of 2 μm and purity of 99.9% (Ningxia Beifang High-Tech Co., Ltd., China) was used as a sintering aid.

2.2 Preparation

In this study, $(Hf_{0.2}Zr_{0.2}Ti_{0.2}Nb_{0.2}Ta_{0.2})N$ high-entropy ceramic powder was initially synthesized by a soft mechanochemistry-assisted nitride thermal reduction method [10,20]. For the synthesis, micron-sized powders of HfO_2, ZrO_2, TiO_2, Nb_2O_5, Ta_2O_5, and Si_3N_4 as raw materials were mixed at a stoichiometric ratio of 2 : 2 : 2 : 1 : 1 : 10. The mixture was then ground in a SP-0.5 high-energy-density stirred bead mill (Shenzhen Sanxing Feirong Machinery Co., Ltd., China) with 0.8–1.0 mm ZrO_2 beads as the grinding medium at a loading volume percentage of 65 vol% and a rotational speed of 1800 r/min for 5 h. Afterwards, the ground mixture was dried and sintered in a HC-ZKSJ-002S vacuum pressureless sintering furnace (Zhuzhou Hechuang Medium and High-Frequency Equipment Co., Ltd., Japan) in an Ar atmosphere with a heating rate of 8 °C/min at 1800 °C for 1 h, thus obtaining submicron-sized high-entropy nitride ceramic powder of $(Hf_{0.2}Zr_{0.2}Ti_{0.2}Nb_{0.2}Ta_{0.2})N$ with a size of 0.2–0.5 μm. Note that the area around the graphite crucible was coated with a layer of graphite paper, and a graphite fiber blanket was used as a cover to absorb SiO produced during the reaction, as SiO can react with graphite fibers to form SiC at high temperatures [10].

For the fabrication of high-entropy nitride bulk composite ceramics, submicron-sized high-entropy nitride ceramic powder was first mixed in deionized water with different mass contents of micron-sized silicon carbide (SiC) powder (i.e., 0, 2.5, 5.0, 7.5, 10.0, 12.5, 15.0, and 20.0 wt%). The mixed slurries were ground and dispersed in a stirred bead mill at 1200 r/min for 3 h. Milling during raw material processing was performed to achieve homogeneous mixing of the powders. The slurries were dried, pressed into discs 20 mm in diameter and 3 mm in thickness, and sintered in a SPS-4 SPS furnace (Shanghai Chenhua Electric Co., Ltd., China). The sintering process was performed initially at a rate of 120 °C/min to 1600 °C while the pressure was increased to 30 MPa for 14 min and then at a rate of 100 °C/min to 1900, 2000, and 2100 °C while the pressure was increased to 40 MPa for 19, 20, and 21 min, respectively. The samples sintered at different temperatures and time were held at the final temperature and pressure for 8 min, resulting in high-entropy nitride composite bulk ceramics of $(Hf_{0.2}Zr_{0.2}Ti_{0.2}Nb_{0.2}Ta_{0.2})N$/SiC.

Figure 1 shows the experimental flowchart for preparing the high-entropy nitride composite bulk ceramics of $(Hf_{0.2}Zr_{0.2}Ti_{0.2}Nb_{0.2}Ta_{0.2})N$/SiC.

2.3 Characterizations

The phase composition of the prepared samples was analyzed by an X-ray diffractometer (XRD; XRD-6000, Shimadzu Co., Japan). The morphology of the samples was determined by a field emission scanning electron microscope (SEM; Sigma55, Zeiss Co., Ltd., Germany), and the grain size was measured with the Nano Measurer software (Shenzhen Nayan Technology Co., Ltd., China). The crystal structure was analyzed via a transmission electron microscope (TEM; Talos F200X, FEI Co., USA). The particle size and size distribution of the raw material mixtures and synthesized powders were determined by a laser diffraction particle size analyzer (Bettersize 2000, Dandong Bettersize Instruments Ltd., China). The bulk density (ρ_b, g/cm^3) of the ceramics was measured via Archimedes' principle, and the theoretical density (ρ_T, g/cm^3) was calculated from the lattice parameters obtained via XRD [1]. The relative density (R_w) can be determined by Eqs. (1)–(3):

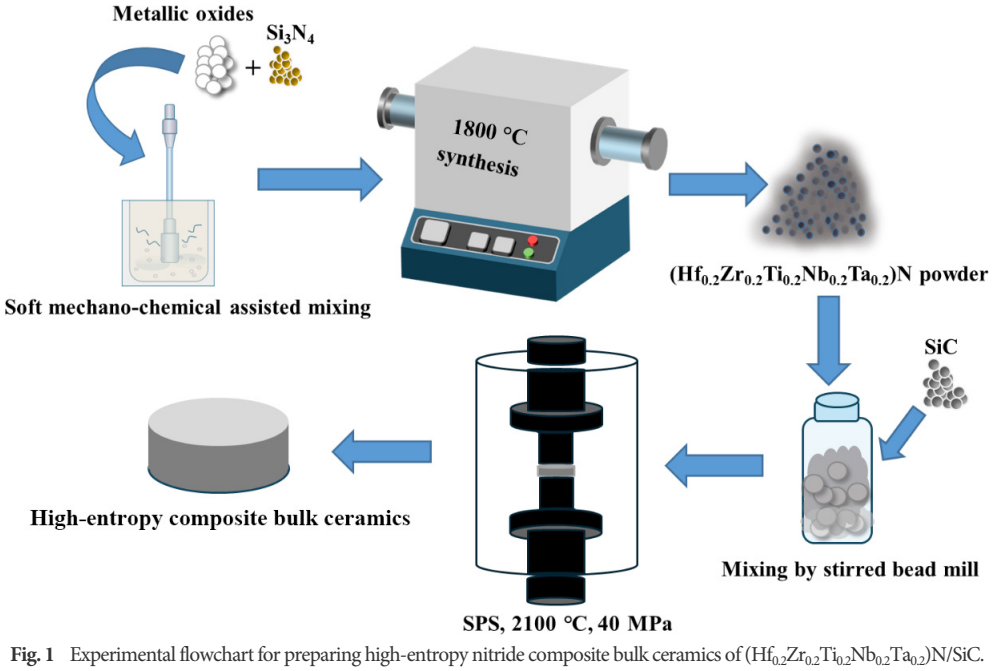

Fig. 1 Experimental flowchart for preparing high-entropy nitride composite bulk ceramics of $(Hf_{0.2}Zr_{0.2}Ti_{0.2}Nb_{0.2}Ta_{0.2})N$/SiC.

$$\rho_b = \frac{\rho_0 m_1}{m_3 - m_2} \quad (1)$$

$$\rho_T = \frac{MZ}{N_A a^3} \quad (2)$$

$$R_w = \frac{\rho_b}{\rho_T} \times 100\% \quad (3)$$

where m_1, m_2, and m_3 are the dry weight, the wet weight, and the weight in water (g) of the sample; ρ_0 is the density of distilled water (g/cm^3); a is the lattice constant (nm); Z is the number of molecules in a single cell; M is the molecular molar mass; N_A is Avogadro constant, with a value of 6.02×10^{23}. The relative density of composite bulk ceramics with different SiC particle contents can be calculated by Eq. (4):

$$R_{w(C)} = (1 - X)R_{w(H)} + XR_{w(S)} \quad (4)$$

where $R_{w(C)}$ is the relative density of the composite bulk ceramics; $R_{W(H)}$ is the relative density of $(Hf_{0.2}Zr_{0.2}Ti_{0.2}Nb_{0.2}Ta_{0.2})N$ high-entropy ceramics; $R_{w(s)}$ is the relative density of SiC; X is the content of SiC particles.

The microhardness and fracture toughness were determined with a microhardness tester (hv-30bz, Taylor Instrument Technology Co., Ltd., China). The load was 98 N, and the loading time was 10 s. The fracture toughness (K_{IC}) is calculated as Eq. (5) [21]:

$$K_{IC} = P\left(\pi\left(\frac{C_1 + C_2}{4}\right)\right)^{-\frac{3}{2}}(\arctan\beta) \quad (5)$$

where P is the load (N); C_1 and C_2 are the lengths of the crack diagonals (m); β is half an indenter angle, which is 68°.

The bending strength (σ_f), which was measured by an universal testing machine (CMT5305, MTS Industrial Systems Co., Ltd., China) based on a three-point bending method, is calculated by Eq. (6):

$$\sigma_f = \frac{3PL}{2bh^2} \quad (6)$$

where P is the load; L is the span; b and h are the width (mm) and height (mm) of the sample, respectively.

For characterizations, eight points of each sample were measured, thereby obtaining the average value with the standard deviation calculated.

3 Results and discussion

3.1 High-entropy composite bulk ceramic

Figure 2(a) shows the XRD patterns of $(Hf_{0.2}Zr_{0.2}Ti_{0.2}Nb_{0.2}Ta_{0.2})N$ (HEN) bulk ceramics sintered at different temperatures. Clearly, the peak intensity of the XRD patterns increases as the sintering temperature increases, indicating that the crystallinity of the bulk ceramics is improved at higher sintering temperatures. As shown in Figs. 2(b) and 2(c), the average grain size of the bulk ceramics increases with increasing sintering temperature. At sintering temperatures of 1900 or 2000 °C, most of the internal pores are intra-granular. At 2100 °C, however, the porosity decreases, and most of the pores are located at the grain boundaries, indicating that the sintering process of high-entropy bulk ceramics is not complete at 1900 or 2000 °C. At 2100 °C, abnormal grain growth occurs, and the average grain size is larger, indicating that the sintering process can be completed at 2100 °C. Table 1 shows the characteristic sizes of d_{50} and d_{90} for the unground, ground, and synthesized powders (d_{50} and d_{90} represent the corresponding particle size when the cumulative particle size distribution percentage of the sample reaches 50% and 90%, respectively).

Figure 3 shows the XRD patterns and SEM images of HEN–SiC high-entropy composite bulk ceramics sintered at 2100 °C. The XRD patterns do not contain diffraction peaks of SiC, likely due to the overlap of SiC peaks with the diffraction peak (111) of HEN. The SEM images reveal that SiC particles are dispersed at the grain boundaries of the bulk ceramics, significantly altering the grain size of the ceramic matrix and reducing its porosity. The bulk ceramics without SiC particles exhibits numerous voids, indicating incomplete densification (Fig. 3(b)). However, the porosity of the bulk ceramics with an appropriate amount of SiC particles (i.e., ≤ 10 wt%) noticeably

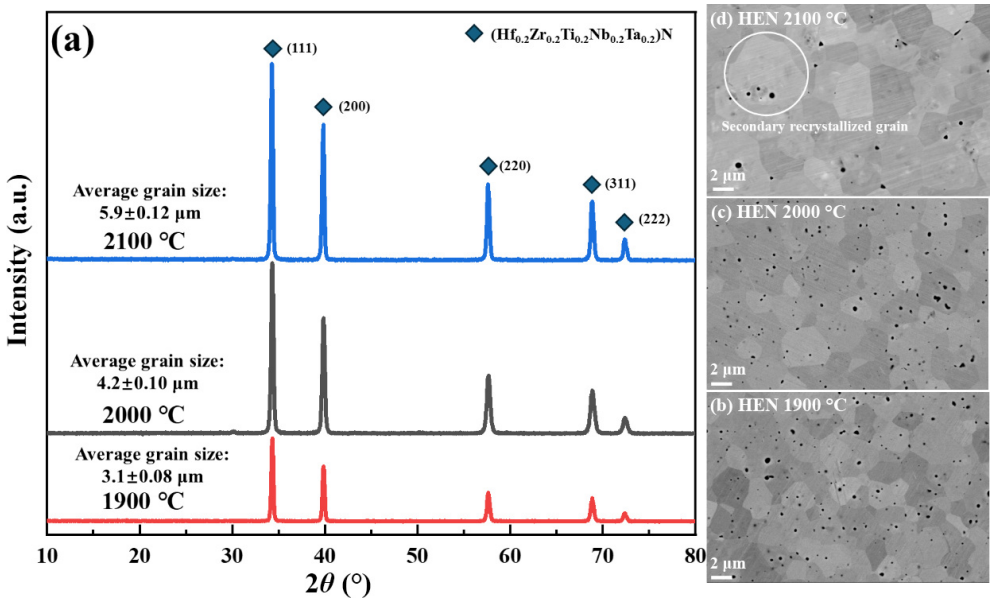

Fig. 2 (a) XRD patterns and average grain sizes and (b–d) SEM images of HEN bulk ceramics sintered at different temperatures.

Table 1 Characteristic sizes (d_{50} and d_{90}) of unground, ground and synthesized powders

High-entropy powder	Unground	Ground	Synthesized
Particle size, d_{50} (μm)	1.832±0.131	0.933±0.062	0.755±0.102
Particle size, d_{90} (μm)	10.583±0.316	8.265±0.103	1.336±0.116

decreases. At a SiC particle content of 10 wt%, SiC particles are well dispersed and distributed uniformly in the bulk ceramics. Note that SiC particles begin to agglomerate, thus forming some clusters in the matrix as the SiC particle content further increases (i.e., 12.5, 15.0, and 20.0 wt%) (Figs. 3(g)–3(i)). This agglomeration negatively affects the performance (i.e., densification and mechanical properties) of the composite bulk ceramics. As shown in Figs. 3(a) and 3(d), some phases with gray contrast appear due to the excessively rapid growth rate of ceramic grains, which leads to the formation of pits at the grain edges. This causes a small number of crystals to grow irregularly in the pits, forming grain clusters that exhibit different contrasts in the SEM images (Fig. 3).

Table 2 shows the cell parameters and average grain sizes of composite bulk ceramics without and with different SiC particle contents sintered at 2100 °C. As indicated in Table 2, the average grain size of bulk ceramics decreases as the unit cell parameters increases. The cell parameters of composite bulk ceramics increase with increasing SiC particle content. However, at greater SiC particle contents (i.e., 12.5, 15.0, and 20.0 wt%), the rate of cell parameter decreases, which aligns with the average grain size as the SiC particle content increases. Additionally, the effect of the addition of SiC particles on the inhibition of the grain growth of the bulk ceramics is dominant at SiC particle contents ranging from 0 to 10.0 wt%. However, when the SiC particle content exceeds 10.0 wt%, there is little change in the grain size. This is because the excessive SiC particles in the composite bulk ceramic begin to agglomerate, thus affecting grain growth.

3.2 Relative density

The main objective of this study was to investigate the effects of SiC particles on the densification behavior of composite ceramics in addition to mechanical properties, and the final relative density of the bulk ceramics was characterized. Figure 4 shows the density data of the bulk ceramics without and with different contents of SiC particles sintered at 2100 °C. When the theoretical density of SiC is 3.20 g/cm^3, the theoretical densities of the bulk ceramics with SiC particle contents of 2.5, 5.0, 7.5, 10.0, 12.5, 15.0, and 20.0 wt% are 9.4575, 9.2971, 9.1366, 8.9762, 8.8158, 8.6553, and 8.3344 g/cm^3, respectively, based on the cell parameters (Table 2). Clearly, the relative density of the bulk ceramic without SiC particles is relatively low (i.e., 93.08%±0.13%). The relative density increases from 93.08%±0.13% to 99.12±0.12% as the SiC particle content in the bulk ceramic increases from 0 to 10.0 wt%. However, the relative density of the bulk ceramics decreases as the SiC particle content further increases (i.e., ≥ 12.5 wt%), and the relative density decreases to 92.31%±0.12% when the SiC particle content is 20.0 wt%. At an optimum SiC particle content of 10.0 wt%, SiC particles disperse evenly, and the particles are tightly packed, which results in a low porosity and prevents abnormal grain growth, thus leading to the maximum relative density. At a lower content of SiC particles (< 10 wt%), the inhibitory effect of SiC particles on grain growth is not sufficient, so the relative density does not increase significantly. However, at a greater SiC particle content of 15.0 or 20.0 wt%, SiC particles start to form some clusters, causing uneven dispersion (Figs. 3(h) and 3(i)), which results in a decrease in the relative density (i.e., 96.33%±0.13% and 92.31%±0.12%).

Since no liquid phase occurs during the sintering of composite bulk ceramics, the densification behavior can be analyzed based on the solid-state sintering theory [22]. Figures 5(a) and 5(b) show the sintering behaviors of bulk ceramics without and with the optimum SiC particle content of 10.0 wt%. According to the theory of solid-state sintering [23,24], particle rearrangement occurs, forming sintering necks between particles, and the distance between particles begins to decrease in the initial stage of sintering. In this stage, the pressure head of the sintering furnace starts to move down slowly from the sintering behavior of bulk

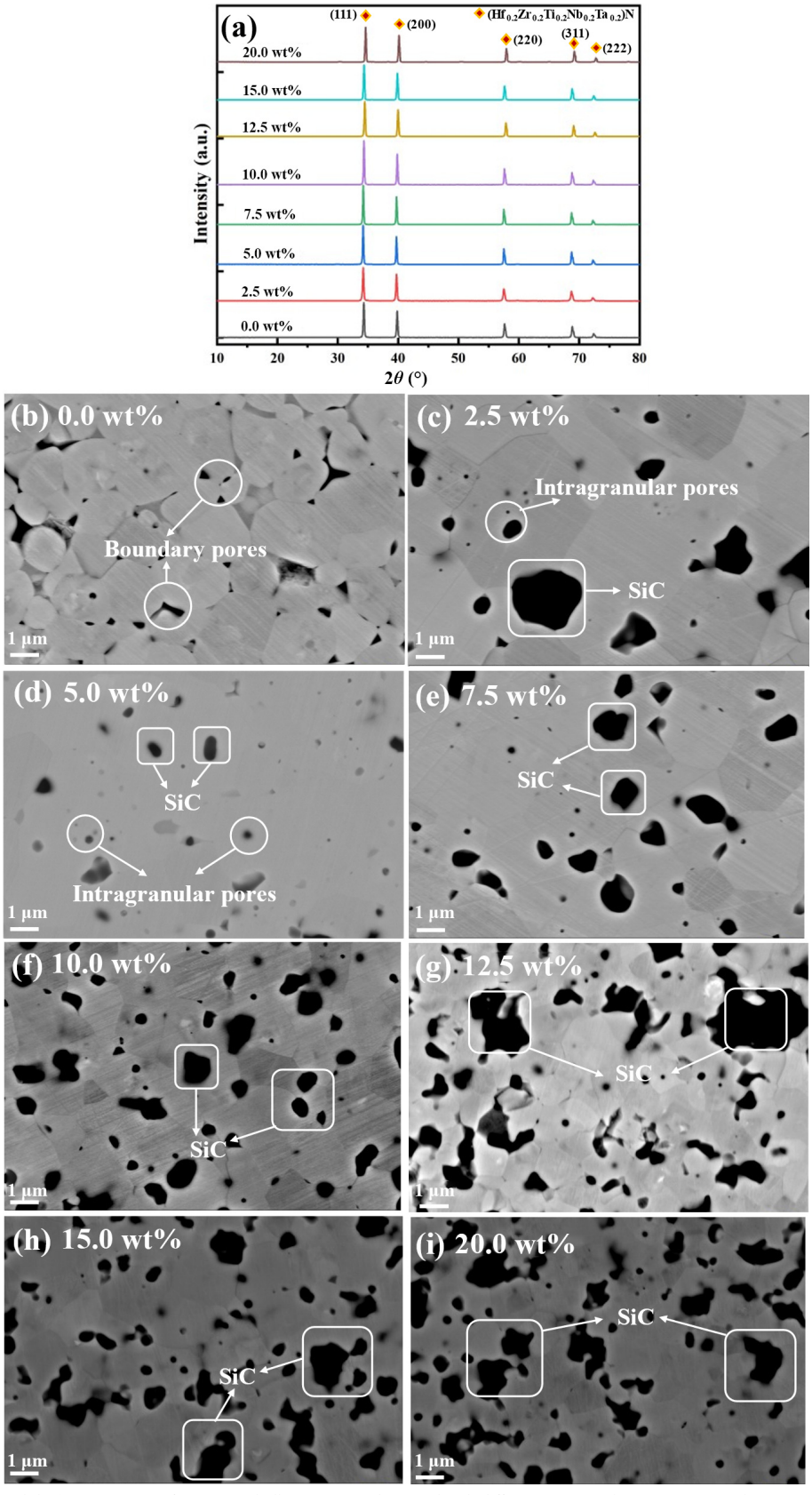

Fig. 3 (a) XRD patterns and (b–i) SEM images of composite bulk ceramics without and with different SiC particle contents sintered at 2100 °C (pores are marked with roundels).

ceramics without and with a SiC particle content of 10.0 wt%, and there is little difference between the two cases at the initial sintering temperatures, indicating that the addition of SiC particles in the ceramic matrix does not reduce the sintering temperature. The second stage of sintering for both samples begins at 1900 °C. The vacuum level during the sintering of the bulk ceramics

Table 2 Cell parameters and average grain sizes of composite bulk ceramics without and with different SiC particle contents sintered at 2100 °C

SiC particle content (%)	$a = b = c$ (Å)	$\alpha = \beta = \gamma$ (°)	Average grain size (μm)
0.0	4.4952	90	6.50±0.12
2.5	4.5011	90	5.60±0.18
5.0	4.5082	90	4.80±0.21
7.5	4.5133	90	3.30±0.16
10.0	4.5186	90	2.10±0.10
12.5	4.5212	90	1.90±0.11
15.0	4.5236	90	1.80±0.09
20.0	4.5255	90	1.60±0.12

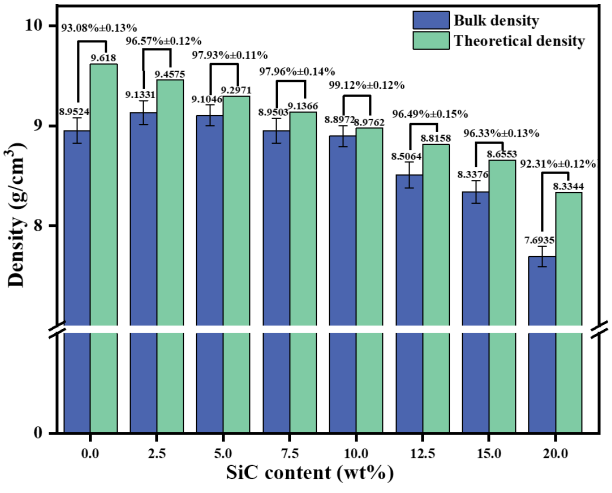

Fig. 4 Density data of composite bulk ceramics without and with different SiC particle contents sintered at 2100°C.

without SiC particles is higher than that of the composite bulk ceramics with a SiC particle content of 10.0 wt%, indicating that less gas is released during the sintering of the bulk ceramics without SiC particles. This is due to the larger average grain size and greater growth rate of ceramics (Fig. 5(c)). During the coalescence and growth of grains, the gas is encapsulated, resulting in an increase in the number of intragranular pores. The average grain size of the bulk ceramic matrix decreases, and the growth rate slows down as as the SiC particle content increases (Fig. 5(c)). This avoids the encapsulation of pores during grain coalescence, allowing more gas to be released, thereby lowering the vacuum level during sintering. Figures 5(d) and 5(e) show the fracture surfaces of the bulk ceramics without and with SiC particle content of 10.0 wt% sintered at 2000 °C, corresponding to the second stage of sintering. The bulk ceramic in the absence of SiC particles clearly has larger overall grain sizes and numerous intragranular pores, indicating that many pores are encapsulated during grain coalescence. In contrast, the composite bulk ceramics with SiC particle content of 10.0 wt% has a smaller overall grain size with some reduced intragranular pores, indicating that the reduction in the grain size and growth rate can effectively prevent the encapsulation of pores during grain growth, thereby inhibiting the formation of intragranular pores. At the end of the second stage of sintering and the beginning of the third stage, the displacement rate of the pressure head during the sintering of the bulk ceramics without SiC particles increases. This is due to the occurrence of abnormal grain growth in the bulk ceramics, leading to an increase in the average grain size, which is detrimental to the densification of the bulk ceramics. In the third stage of sintering, the displacement rate of the pressure head for the composite bulk ceramics with SiC particle content of 10.0 wt% is lower, and the vacuum level increases and then stabilizes, indicating normal grain growth, gradual elimination of pores, and a trend towards complete densification.

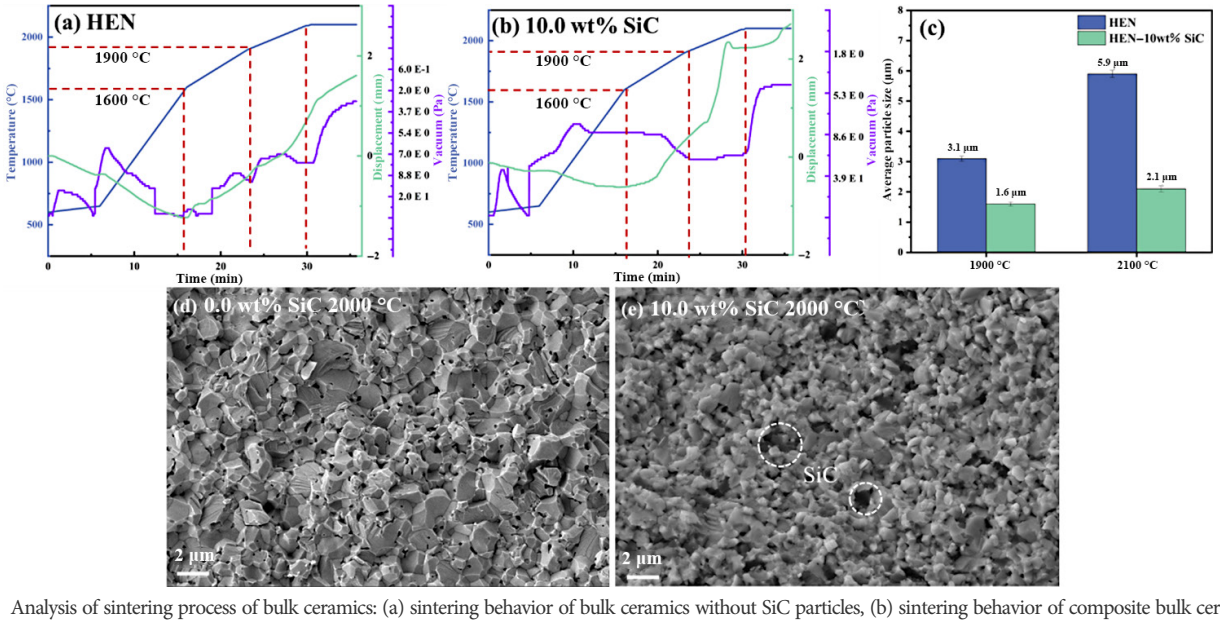

Fig. 5 Analysis of sintering process of bulk ceramics: (a) sintering behavior of bulk ceramics without SiC particles, (b) sintering behavior of composite bulk ceramics with SiC particle content of 10.0 wt%, (c) average grain sizes of bulk ceramics without and with SiC particle content of 10.0 wt%, and fracture surfaces of bulk ceramics (d) without SiC particles and (e) with SiC particle content of 10.0 wt% sintered at 2000°C.

Based on the Johnson-Mehl equation [25], the grain size (d) can be expressed as Eq. (7):

$$d = k \times \left(\frac{G}{N}\right)^{\frac{1}{4}} \tag{7}$$

where G is the growth rate; N is the nucleation rate; k is a constant. It is evident that some factors (e.g., sintering temperature, addition of a sintering aid or second phase) affecting G and N can affect the grain size. SiC particles are added to the ceramic matrix as a second phase, which can promote heterogeneous nucleation and increase the nucleation rate. Additionally, SiC particles have an adsorption effect in the grain boundary region, forming Cottrell atmospheres, which exert a pinning effect on the grain boundaries (i.e., Zener pinning, Fig. 6) [26,27]. This slows down grain boundary migration, obstructs mass diffusion, and reduces grain growth rate. Under the combined influence of these factors, the grain size of ceramics significantly reduces, and the decreased growth rate prevents the encapsulation of pores during grain coalescence, greatly reducing the occurrence of enclosed intragranular pores.

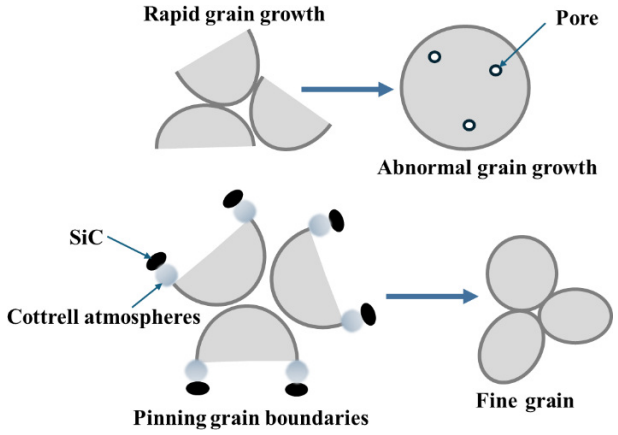

Fig. 6 Schematic of Zener pinning.

Clearly, the pinning effect of SiC particles at an appropriate content (i.e., 10.0 wt%) on the grain boundaries refines the grain size of the ceramics, slows down the growth rate of the ceramic matrix grains, primarily affects the second and third stages of sintering, reduces the occurrence of intragranular pores, and prevents secondary recrystallization, thus enhancing the relative density of the ceramics. When the SiC particle content is less than 10.0 wt%, however, it does not have a sufficient effect on the grain refinement, leading to a lower relative density. When the SiC particle content is greater than 10.0 wt%, the SiC particles begin to adhere and agglomerate, and the bonding between SiC clusters and matrix ceramic grains becomes poor, resulting in a decrease in the relative density of ceramics.

3.3 Mechanical properties

Figure 7 shows the mechanical properties (i.e., hardness, fracture toughness, and flexural strength) of bulk ceramics without and with different SiC particle contents sintered at 2100 °C. The hardness clearly increases from 19.16±0.56 to 23.34±0.67 GPa; the fracture toughness increases from 3.78±0.09 to 4.35±0.13 MPa·m$^{1/2}$; the bending strength increases from 335±11 to 409±11 MPa as the SiC particle content in the bulk ceramic increases from 0 to

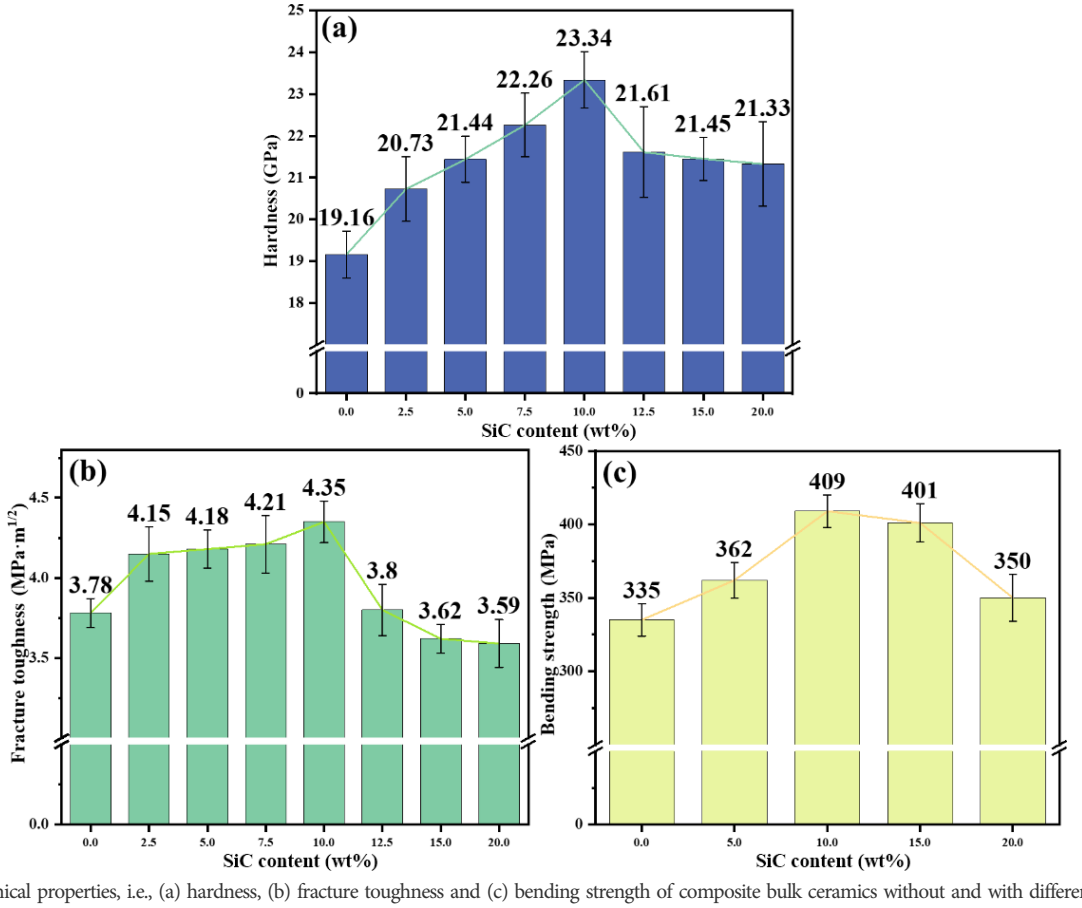

Fig. 7 Mechanical properties, i.e., (a) hardness, (b) fracture toughness and (c) bending strength of composite bulk ceramics without and with different SiC particle contents sintered at 2100 °C.

10.0 wt%. However, as the SiC particle content further increases to 12.5 wt% or more, the mechanical properties of the composite bulk ceramics decrease, particularly the fracture toughness. At a SiC particle content of 20.0 wt%, the fracture toughness decreases to 3.59±0.15 MPa·m$^{1/2}$, which is even lower than that of the bulk ceramics without SiC particles (i.e., 3.78±0.09 MPa·m$^{1/2}$). The superior mechanical properties of ($Hf_{0.2}Zr_{0.2}Ti_{0.2}Nb_{0.2}Ta_{0.2}$)N/SiC high-entropy composite bulk ceramics can be obtained at an optimum SiC particle content of 10.0 wt%.

In addition to the increased relative density, the improvement in the mechanical properties of the bulk ceramics is also attributed to the introduction of SiC particles in the ceramic matrix at an appropriate or optimum content (i.e., 10.0 wt%). Clearly, the appropriate addition of SiC particles into the matrix can refine the ceramic grains, and the relationship between material strength and grain size can be described by the Hall-Petch equation (Eq. (8)) [28–30]:

$$\sigma_s = \sigma_0 + kd^{-\frac{1}{2}} \tag{8}$$

where σ_s is the yield strength of the material; σ_0 is the yield strength of a single crystal; k is the Hall-Petch slope that indicates the strengthening contribution of grain boundaries; d is the average grain size. Figure 8 shows SEM images of the fracture morphology of the bulk ceramics without and with different SiC particle contents. It is evident that SiC particles significantly inhibit the grain growth of the matrix. As the amount of SiC particles increases, the grain size of the high-entropy ceramic matrix significantly decreases, resulting in an increased number of grains and grain boundaries per unit volume. These grain boundaries effectively impede dislocation movement within the matrix, thereby enhancing the resistance of the material to deformation. In addition to using SiC particles as a sintering aid, SiC particles can also be considered secondary phases dispersed at the grain boundaries of high-entropy ceramics. The presence of the dispersed secondary phase hinders the advance of the crack tip during crack propagation. This causes the crack to bend along SiC particles, obstructing the main crack growth. Moreover, residual compressive stresses develop around the interfaces between SiC particles as a dispersed phase and the high-entropy ceramic matrix, causing crack deflection when these particles are present. This increases the energy required for crack propagation, thus improving the resistance of ceramics to crack growth. Figure 8 also shows numerous dimples, indicating that the fracture mode of the bulk ceramics is primarily intergranular fracture (Figs. 8(c) and 8(d)), exhibiting a pull-out mechanism characteristic of particle dispersion toughening.

Figure 9 shows SEM images of SiC particles toughened in the composite bulk ceramics with a SiC particle content of 10.0 wt% sintered at 2100 °C. As SiC particles fill in the HEN matrix during sintering at high temperatures, the sharp and small edged ends of SiC particles in the HEN matrix may contact and adhere, undergoing a riveting phenomenon to form SiC particle chains (Fig. 9(a)) [18]. Additionally, as shown in Fig. 9(b), SiC particles may form a lamellar structure in inter-HEN particle gaps. In addition to the effect of fine grains, lamellar/chain structures may also enhance the pull-out mechanism, further improving the toughness of the composite bulk ceramic [31,32]. SiC particles can contribute to the toughening effect through the pull-out mechanism. Therefore, the introduction of SiC particles in the high-entropy bulk ceramic matrix can enhance toughening, primarily through the synergistic effects of second-phase pull-out and crack deflection. As the SiC particle content further increases (i.e., 12.5, 15.0, and 20.0 wt%), SiC particles begin to agglomerate and form some clusters, leading to a decline in the mechanical properties of the composite bulk ceramics, especially the fracture toughness (Fig. 7). Figure 10 shows SEM images and energy

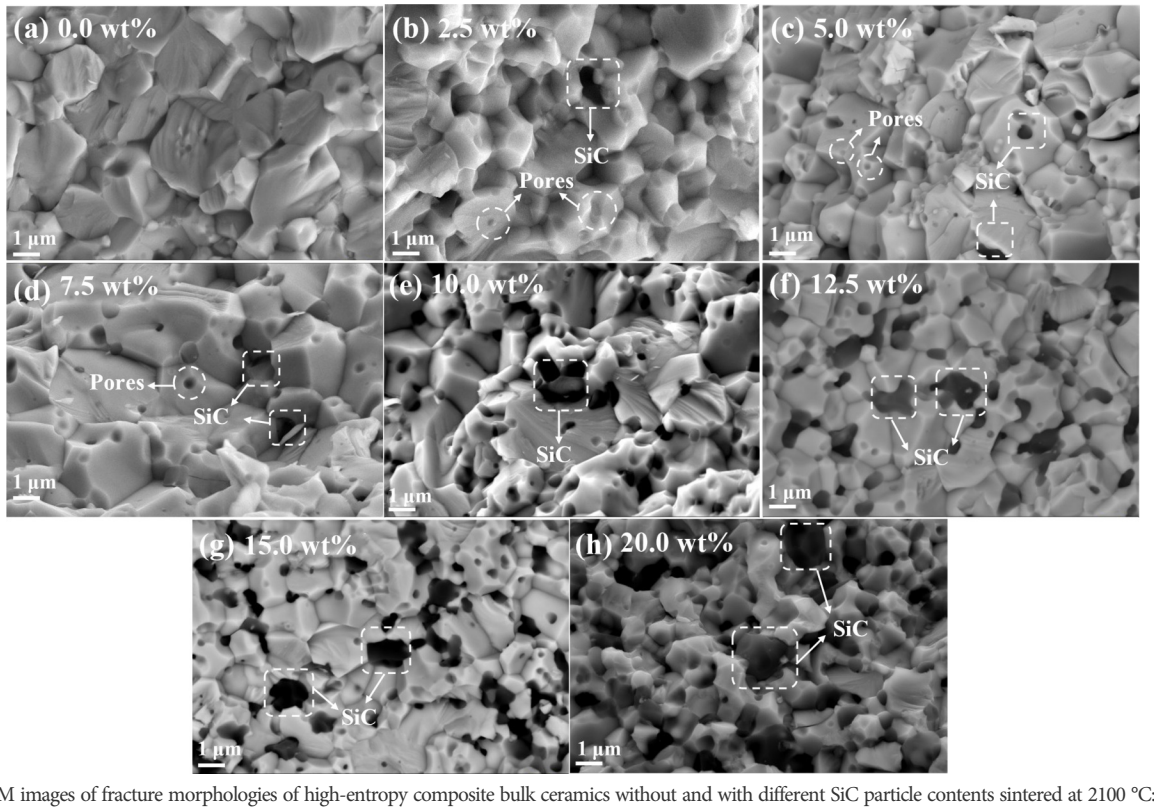

Fig. 8 SEM images of fracture morphologies of high-entropy composite bulk ceramics without and with different SiC particle contents sintered at 2100 °C: (a) HEN without SiC particles, (b) 2.5 wt%, (c) 5.0 wt%, (d) 7.5 wt%, (e) 10.0 wt%, (f) 12.5 wt%, (g) 15.0 wt%, and (h) 20.0 wt%.

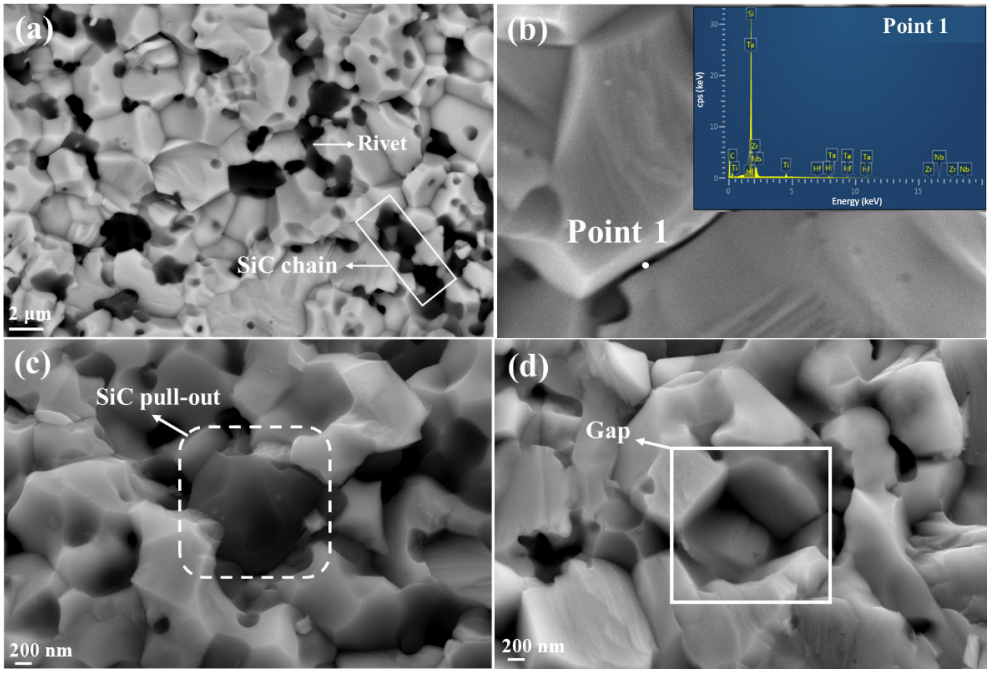

Fig. 9 SEM images of SiC particles toughened in high-entropy composite bulk ceramics with SiC particle content of 10.0 wt% sintered at 2100 °C: (a) SiC rivet and SiC chains, (b) SiC lamella in inter-particle gaps, (c) SiC pull-out, and (d) gap.

dispersive X-ray spectroscopy (EDS) mapping of the composite bulk ceramics with different SiC particle contents. Figure 10(b) clearly shows that SiC particles are uniformly dispersed and smaller in size at an optimum SiC particle content of 10.0 wt%. When the SiC particle content is either below or above 10.0 wt%, the dispersion of SiC particles becomes poor, resulting in particle agglomeration (Figs. 10(a), 10(c), and 10(d)).

Figure 11 shows the TEM images and EDS mappings of the high-entropy composite bulk ceramics with an optimum SiC particle content of 10.0 wt%. Clearly, the TEM images include both bright and dark phases due to the different electron scattering abilities of various elements. The EDS point analysis indicates that the bright phase is silicon carbide (SiC), and the dark phase is HEN (Fig. 11(a)). In addition, there is also an overlap phenomenon in the elemental distribution because the characteristic X-ray photon energies of Si and Ta are similar (Fig. 10). As shown in Fig. 11(b), SiC particles are dispersed within the HEN matrix, and no solid solution is formed between the two phases. This indicates that no solid solution diffusion occurs during the sintering or diffusion process. Figure 12 shows the high-resolution TEM (HRTEM) images of the high-entropy composite bulk ceramics with an optimum SiC particle content of 10.0 wt%. Based on the lattice fringe analysis, the interplanar spacings of SiC and HEN are 0.183 and 0.237 nm, respectively. As shown in Fig. 12(a), SiC and HEN are tightly bonded without any transitional layer, forming an intense interface. This tight bonding means that more energy is required for SiC particles to detach from the matrix, thus enhancing the pull-out toughening effect. Telectron diffraction analysis reveals that SiC and HEN have a hexagonal structure and a cubic structure, respectively, with well-ordered atomic arrangements and good crystallinity (Figs. 12(b) and 12(c). As shown in Fig. 12(d), the inverse fast Fourier transform (IFFT) of the area near the SiC and HEN interface reveals a significant amount of distortion in the vicinity of the interface. These distortions can greatly hinder crack propagation, causing the cracks to deflect when passing near SiC particles, thereby enhancing the fracture resistance of the bulk ceramics. Clearly, the uniform dispersion of SiC particles at an appropriate content creates more interfaces, significantly improving the fracture toughness of the bulk ceramics. This is also one of the reasons why the mechanical properties of bulk ceramics decrease when SiC particles agglomerate to form clusters at high SiC particle contents (i.e., > 10.0 wt%).

In this work, SiC particles at an appropriate amount are used as additives to improve the fracture toughness of $(Hf_{0.2}Zr_{0.2}Ti_{0.2}Nb_{0.2}Ta_{0.2})N$ bulk ceramics. However, several challenges remain for large-scale production. As is known, ensuring a uniform distribution of SiC particles during large-scale mixing is difficult, and particle agglomeration occurs at a high SiC particle content, which directly affects the relative density and mechanical properties of the composite bulk ceramics. Additionally, the SPS sintering method used in this study is suitable for small-scale experiments rather than large-scale production, restricting its efficiency in producing structural components with various shapes.

4 Conclusions

High-entropy composite bulk ceramics of $(Hf_{0.2}Zr_{0.2}Ti_{0.2}Nb_{0.2}Ta_{0.2})N$/silicon carbide (HEN/SiC) were prepared via SPS at 2100 °C with submicron-sized single-phase HEN powder as raw materials and SiC particles as a sintering aid. The effects of the SiC particle content on the grain size, grain growth rate, relative density, and mechanical properties (i.e., bending strength, Vickers hardness and fracture toughness) of composite bulk ceramics were investigated; the densification process, crack propagation behavior, and fine-grained toughening mechanism of SiC as a secondary phase of the bulk ceramics were analyzed. The results showed that the high-entropy composite bulk ceramic with a SiC particle content of 10.0 wt% exhibited the optimum mechanical properties (i.e., Vickers hardness of 23.34±0.67 GPa, fracture toughness of 4.35±0.13 MPa·$m^{1/2}$, and bending strength of 409±11 MPa) compared with those of the ceramics without SiC particles (i.e., Vickers hardness of

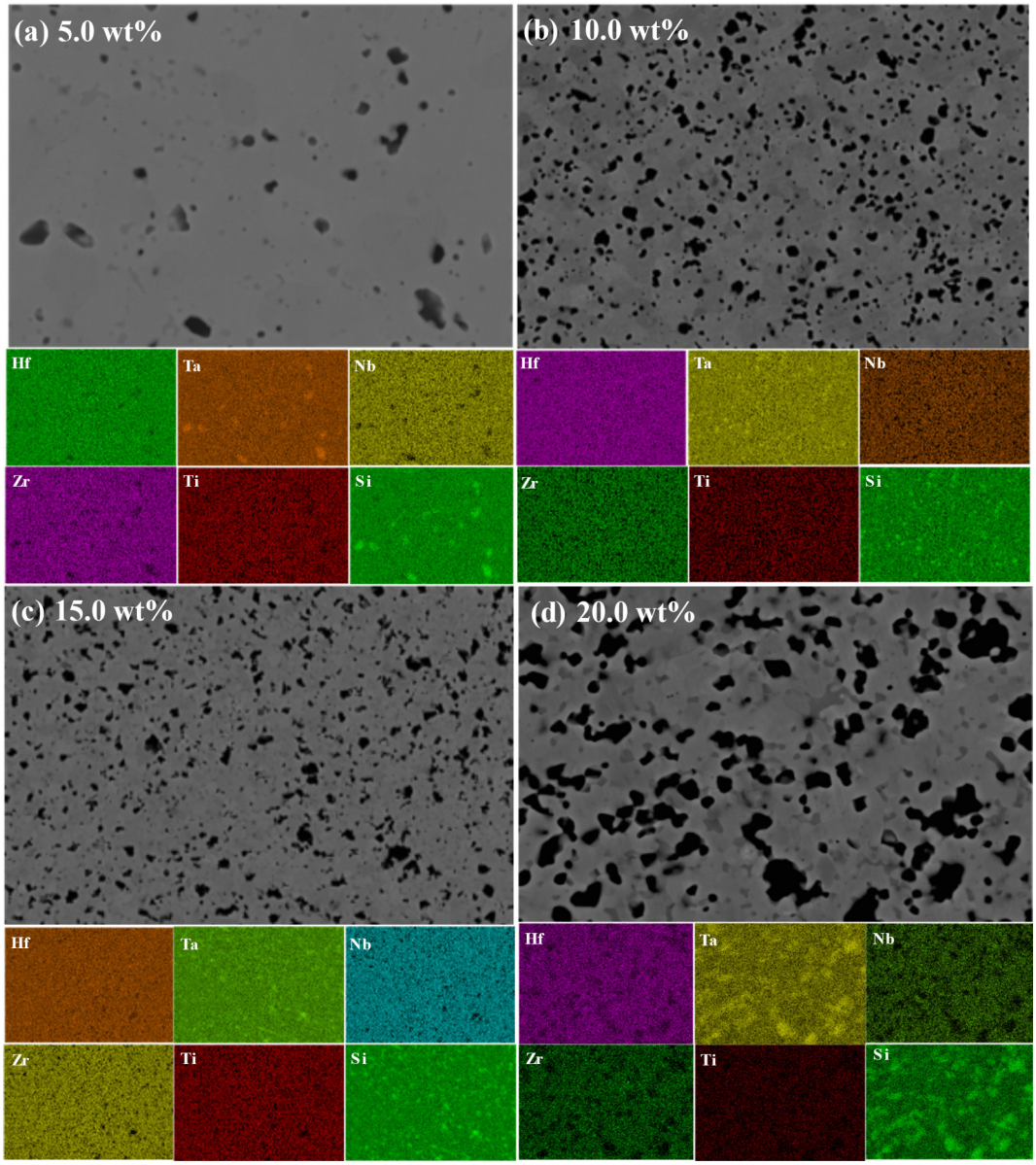

Fig. 10 SEM images and EDS mappings of composite bulk ceramics with different SiC particle contents sintered at 2100 °C: (a) 5.0 wt%, (b) 10.0 wt%, (c) 15.0 wt%, and (d) 20.0 wt%.

19.16±0.56 GPa, fracture toughness of 3.78±0.09 MPa·m$^{1/2}$, and bending strength of 335±11 MPa). The SiC particles could agglomerate to form clusters as the SiC particle content exceeded 10.0 wt%, weakening the grain boundaries and reducing the ceramic performance. According to the analysis of the densification process, SiC pinning the grain boundaries of high-entropy bulk ceramics refined the grains and inhibited the grain growth, primarily in the second and third stages of sintering. This pinning effect prevented pores from being trapped within the grains during densification. SiC particles at an appropriate content (i.e., 10.0 wt%) distributed at the grain boundaries facilitated the expulsion of intergranular pores, ultimately enhancing the relative density of the bulk ceramics. In addition to the enhanced relative density, the improved mechanical properties of the high-entropy composite bulk ceramic with an optimum SiC particle content of 10.0 wt% were attributed mainly to the refined grain size and the synergistic effect of SiC as a secondary phase impeding crack propagation. SiC could refine the grain size of the matrix ceramics, increasing the number of grain boundaries per unit volume and hindering dislocation movement. SiC particles, as a second phase, could be dispersed among the matrix ceramic grains, causing crack deflection and thus impeding crack propagation. In addition, the pull-out phenomenon of SiC particles occurred due to the presence of fine grains, indicating the presence of a pull-out toughening mechanism within the matrix. Moreover, the lamellar/chain structure of SiC particles at an appropriate content (i.e., 10.0 wt%) also formed during the sintering process of composite bulk ceramics, further enhancing the pull-out mechanism and improving the fracture toughness of composite bulk ceramics.

In previous studies [6,10], $(Hf_{0.2}Zr_{0.2}Ti_{0.2}Nb_{0.2}Ta_{0.2})N$ high-entropy bulk ceramics sintered via SPS at 2100 °C had a relative density of 94.31%±0.76% or 96.6%±0.31% and a fracture toughness of 3.18±0.16 MPa·m$^{1/2}$. In this study, the addition of SiC particles significantly improved the relative density and fracture toughness of $(Hf_{0.2}Zr_{0.2}Ti_{0.2}Nb_{0.2}Ta_{0.2})N$ high-entropy bulk ceramics (i.e., a relative density of 99.12±0.12% and a fracture toughness of 4.35±0.13 MPa·m$^{1/2}$).

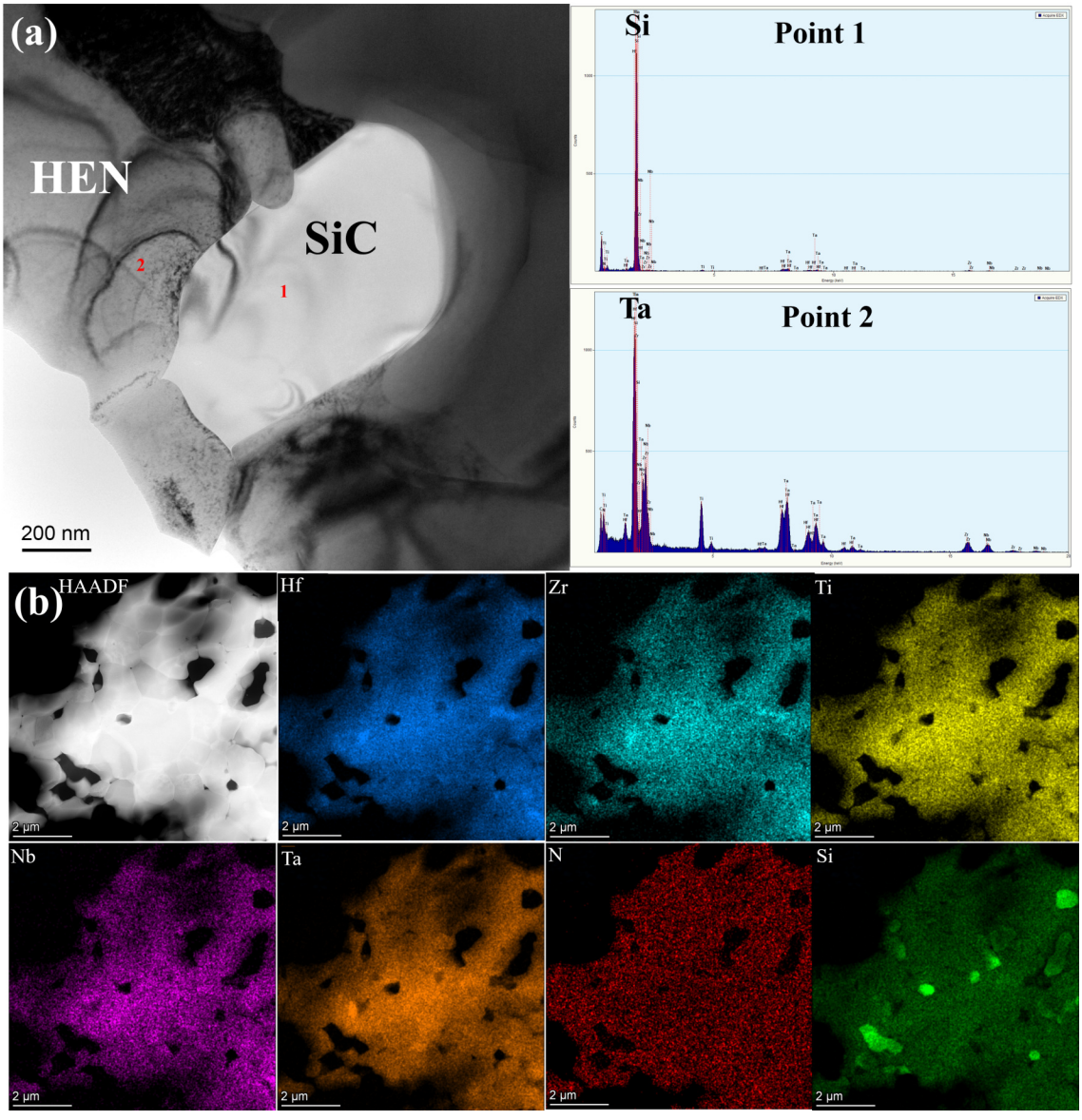

Fig. 11 TEM images and EDS mapping of composite bulk ceramics with SiC particle content of 10.0 wt% sintered at 2100 °C: (a) TEM image, (b) EDS mappings.

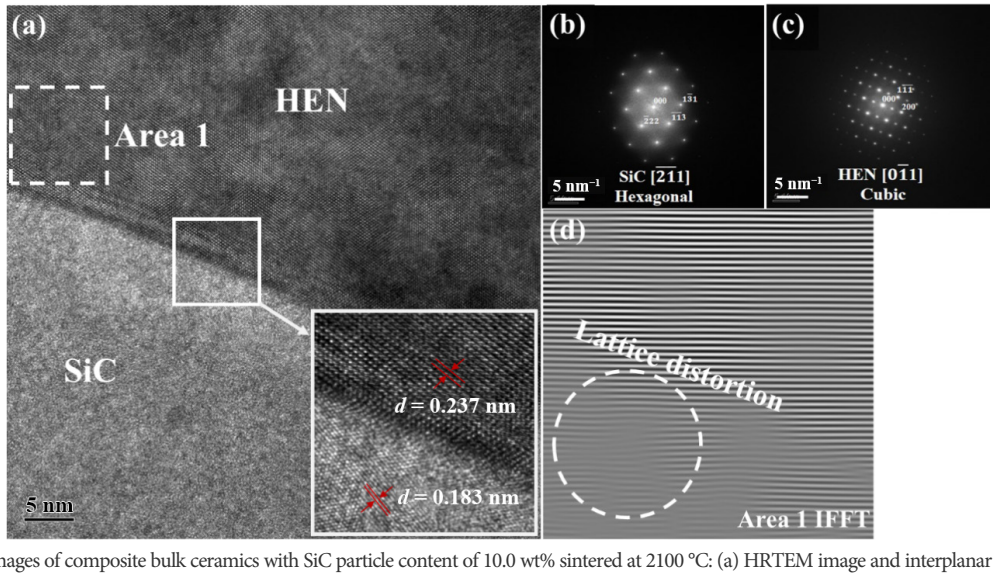

Fig. 12 HRTEM images of composite bulk ceramics with SiC particle content of 10.0 wt% sintered at 2100 °C: (a) HRTEM image and interplanar spacing, (b) electron diffraction pattern of SiC, (c) electron diffraction pattern of HEN, and (d) IFFT of area 1 in (a).

The results indicated that this high-entropy composite bulk ceramic could be used as a promising candidate for applications in aerospace components (i.e., turbine blades and combustion chambers), nuclear reactors (i.e., components exposed) and cutting tools.

Acknowledgements

This work was supported by the National Natural Science Foundation of China (No. U23A20562) and the Graduate Student Innovation Program (No. YCX23109).

Declaration of competing interest

The authors have no competing interests to declare that are relevant to the content of this article.

References

[1] Rost CM, Sachet E, Borman T, *et al.* Entropy-stabilized oxides. *Nat Commun* 2015, **6**: 8485.
[2] Xiang HM, Xing Y, Dai FZ, *et al.* High-entropy ceramics: Present status, challenges, and a look forward. *J Adv Ceram* 2021, **10**: 385–441.
[3] Oses C, Toher C, Curtarolo S. High-entropy ceramics. *Nat Rev Mater* 2020, **5**: 295–309.
[4] Feng L, Fahrenholtz WG, Hilmas GE, *et al.* Synthesis of single-phase high-entropy carbide powders. *Scripta Mater* 2019, **162**: 90–93.
[5] Zhang WM, Zhao B, Xiang HM, *et al.* One-step synthesis and electromagnetic absorption properties of high entropy rare earth hexaborides (HE REB6) and high entropy rare earth hexaborides/borates (HE REB_6/HE $REBO_3$) composite powders. *J Adv Ceram* 2021, **10**: 62–77.
[6] Moskovskikh D, Vorotilo S, Buinevich V, *et al.* Extremely hard and tough high entropy nitride ceramics. *Sci Rep* 2020, **10**: 19874.
[7] Nikolay E, Alexey M, Ivan B, *et al.* Self-propagating high-temperature synthesis of high-entropy ceramic composition $(Hf_{0.25}Ti_{0.25}Cr_{0.25}(FeV)_{0.25})N$. *Mater Lett* 2023, **346**: 134562.
[8] Jin T, Sang XH, Unocic RR, *et al.* Mechanochemical-assisted synthesis of high-entropy metal nitride via a soft urea strategy. *Adv Mater* 2018, **30**: 1707512.
[9] Qu FD, Yuan Y, Yang MH. Programmed synthesis of Sn_3N nanoparticles via a soft chemistry approach with urea: Application for ethanol vapor sensing. *Chem Mater* 2017, **29**: 969–974.
[10] Liu X, Lu YJ, Xu Q, *et al.* Synthesis of (HfZrTiNbTa)N powders via nitride thermal reduction with soft mechano–chemical assistance. *J Adv Ceram* 2023, **12**: 565–577.
[11] Zhou L, Liu JX, Tu TZ, *et al.* Fast grain growth phenomenon in high-entropy ceramics: A case study in rare-earth hexaaluminates. *J Adv Ceram* 2023, **12**: 111–121.
[12] Luo SC, Guo WM, Plucknett K, *et al.* Low-temperature densification of high-entropy (Ti,Zr,Nb,Ta,Mo)C–Co composites with high hardness and high toughness. *J Adv Ceram* 2022, **11**: 805–813.
[13] Zhang Y, Sun SK, Guo WM, *et al.* Optimal preparation of high-entropy boride-silicon carbide ceramics. *J Adv Ceram* 2021, **10**: 173–180.
[14] Zou XG, Ni DW, Chen BW, *et al.* Fabrication and mechanical behavior of 2D-$C_f/Ta_xHf_{1-x}C$–SiC composites by a low-temperature and highly-efficient route. *J Adv Ceram* 2023, **12**: 1961–1972.
[15] Kombamuthu V, Ünsal H, Chlup Z, *et al.* Effect of SiC on densification, microstructure and mechanical properties of high entropy diboride $(Ti_{0.2}Zr_{0.2}Hf_{0.2}Nb_{0.2}Ta_{0.2})B_2$. *J Eur Ceram Soc* 2024, **44**: 5358–5369.
[16] Cheng YY, Zhou L, Liu JX, *et al.* Grain growth inhibition by sluggish diffusion and Zener pinning in high-entropy diboride ceramics. *J Am Ceram Soc* 2023, **106**: 4997–5004.
[17] Lu K, Liu JX, Wei XF, *et al.* Microstructures and mechanical properties of high-entropy $(Ti_{0.2}Zr_{0.2}Hf_{0.2}Nb_{0.2}Ta_{0.2})C$ ceramics with the addition of SiC secondary phase. *J Eur Ceram Soc* 2020, **40**: 1839–1847.
[18] Guo WJ, Hu J, Ye YC, *et al.* Ablation behavior of (TiZrHfNbTa)C high-entropy ceramics with the addition of SiC secondary under an oxyacetylene flame. *Ceram Int* 2022, **48**: 12790–12799.
[19] Rana D, Balani K. Isolating strengthening contributions in multiphase high entropy (Zr–Ta–W–Ti)C–SiC based carbide ceramics. *Int J Refract Met H* 2023, **110**: 106024.
[20] Song WY, Lu YJ, Wang CY, *et al.* Atomic arrangement and mechanical properties of high-entropy nonoxide ceramics simulated via location preference-based disordered random structure. *J Alloys Compd* 2024, **1002**: 175455.
[21] Evans AG, Charles EA. Fracture toughness determinations by indentation. *J Am Ceram Soc* 1976, **59**: 371–372.
[22] Chen RY, Xin JX, Zhan J, *et al.* Effects of novel carbon sources additives on the solid-state sintering behavior and properties of SiC ceramics. *Ceram Int* 2024, **50**: 43082–43088.
[23] Su H, Johnson DL. Master sintering curve: A practical approach to sintering. *J Am Ceram Soc* 1996, **79**: 3211–3217.
[24] Tatami J, Suzuki Y, Wakihara T, *et al.* Control of shrinkage during sintering of alumina ceramics based on master sintering curve theory. *Key Eng Mater* 2006, **317–318**: 11–14.
[25] Fanfoni M, Tomellini M. The Johnson–Mehl–Avrami–Kohnogorov model: A brief review. *Il Nuovo Cimento D* 1998, **20**: 1171–1182.
[26] Smith CS. Grains, phases, and interfaces: An interpretation of microstructure. *Metall Mater Trans A* 2010, **41**: 1064–1100.
[27] Chakrabarti T, Manna S. Zener pinning through coherent precipitate: A phase-field study. *Comput Mater Sci* 2018, **154**: 84–90.
[28] Hall EO. The deformation and ageing of mild steel: III discussion of results. *Proc Phys Soc B* 1951, **64**: 747–753.
[29] Gil Sevillano J, van Houtte P, Aernoudt E. Large strain work hardening and textures. *Prog Mater Sci* 1980, **25**: 69–134.
[30] Petch NJ. The cleavage strength of polycrystals. *J Iron Steel Inst* 1953, **174**: 25–28
[31] Ma XH, Peng HD, Wang SC, *et al.* High-temperature mechanical performances of SiC whisker *in situ* toughened 3DN C/SiC countersunk bolts prepared by chemical vapor infiltration. *Ceram Int* 2024, **50**: 42478–42494.
[32] Liu DW, Yin ZB, Guo FZ, *et al.* Densification, microstructure and properties of α/β-SiAlON ceramic reinforced by SiC whiskers. *Ceram Int* 2024, **50**: 42755–42765.